

# Magnetostructural correlations in $S = 1$ *trans*-[Ni{(OPPh<sub>2</sub>)(EPh<sub>2</sub>)N}<sub>2</sub>(dmsO)<sub>2</sub>], E = S, Se, and related complexes

Eleftherios Ferentinos<sup>a</sup>, Catherine P. Raptopoulou<sup>b</sup>, Vassilis Psycharis<sup>b</sup>, Aris Terzis<sup>b</sup>, J. Krzystek<sup>c,\*</sup>, Panayotis Kyritsis<sup>a,\*</sup>

<sup>a</sup>Inorganic Chemistry Laboratory, Department of Chemistry, National and Kapodistrian University of Athens, 15771 Athens, Greece

<sup>b</sup>NCSR "Demokritos", Institute of Nanoscience and Nanotechnology, 15310 Aghia Paraskevi, Athens, Greece

<sup>c</sup>National High Magnetic Field Laboratory, Florida State University, Tallahassee, FL 32310, USA

## ARTICLE INFO

### Article history:

Received 23 March 2018

Accepted 15 May 2018

Available online 23 May 2018

Dedicated on the occasion of the 65th birthday of Professor Spyros Perlepes, in recognition of his inspiring research in the fields of coordination chemistry and molecular magnetism.

### Keywords:

Nickel

Imidodiphosphinato ligand

X-ray crystallography

EPR spectroscopy

Magnetostructural correlations

## ABSTRACT

In this work, the structural and spectroscopic characterization of *trans*-[Ni{(OPPh<sub>2</sub>)(EPh<sub>2</sub>)N}<sub>2</sub>(dmsO)<sub>2</sub>], E = S, Se, complexes is described. These Ni(II) complexes contain two chelating (O,E) = [(OPPh<sub>2</sub>)(EPh<sub>2</sub>)N]<sup>-</sup> ligands, as well as two dimethyl sulfoxide (dmsO) molecules coordinated via their O atoms. X-ray crystallography studies revealed a highly anisotropic pseudo-octahedral *trans*-NiO<sub>4</sub>E<sub>2</sub> coordination environment, extending the literature dataset of their *trans*-[Ni(O,E)<sub>2</sub>(sol)<sub>2</sub>], sol = dmf, thf, counterparts. Collectively considered, these six complexes contain similar coordination spheres, exhibiting, however, subtle structural differences due to the nature of the donor atom (E) and solvent molecule (sol) coordinated to Ni(II). The spin Hamiltonian parameters of  $S = 1$  *trans*-[Ni(O,Se)<sub>2</sub>(dmsO)<sub>2</sub>], E = S, Se, were accurately determined by high-frequency and -field EPR spectroscopy, applying a methodology already used for *trans*-[Ni(O,E)<sub>2</sub>(sol)<sub>2</sub>], sol = dmf, thf. Magnetostructural correlations are explored between all members of this sub-family of Ni(II) complexes.

© 2018 Elsevier Ltd. All rights reserved.

## 1. Introduction

The so called dichalcogenoimidodiphosphinato type of ligands, R<sub>2</sub>P(E)NHP(E')R'<sub>2</sub> (E, E' = O, S, Se, Te; R, R' = alkyl or aryl peripheral groups), exhibit a rich coordination chemistry towards both main group and transition metal elements, especially in their anionic (E, E') = [R<sub>2</sub>P(E)NP(E')R'<sub>2</sub>]<sup>-</sup> bis-chelating form [1–5]. Among the large number of 3d-metal complexes bearing these ligands, Ni(II) complexes have been shown to exhibit a remarkable structural versatility with respect to both composition and geometry of their first coordination sphere, depending on the nature of the E, E' donor atoms and the R, R' peripheral groups of the ligand. More specifically, bis-chelated, [Ni(S,S)<sub>2</sub>], complexes containing the same peripheral groups (R = R' = Me [6] or iPr [7]) exhibit exclusively tetrahedral NiS<sub>4</sub> coordination spheres. On the other hand, the complex with R = R' = Ph exhibits both tetrahedral [8,9] and square-planar geometries [10], and those with R = Ph and R' = Me [9] or

iPr [11], only the square-planar one. Analogous observations have been made in the case of [Ni(Se,Se)<sub>2</sub>], for which either exclusive square-planar (R = R' = Ph) [12], or both tetrahedral and square-planar [13,14] NiSe<sub>4</sub> (R = R' = iPr) coordination spheres have been observed. The (Te,Te) ligand with R = R' = iPr affords square-planar [Ni(Te,Te)<sub>2</sub>] [13]. On the other hand, the (O,O) ligand with R = R' = Ph affords the dinuclear [Ni<sub>2</sub>(O,O)<sub>4</sub>] complex, but in the presence of dmf, the mononuclear [Ni(O,O)<sub>2</sub>(dmf)<sub>2</sub>] complex has been also isolated [15]. Mixed-donor-atom ligands (O,E) have been shown to form exclusively tetrahedral [M(O,E)<sub>2</sub>] complexes, E = S [16], Se [17], which, in the presence of coordinating solvents, have been converted to pseudo-octahedral *trans*-[M(O,E)<sub>2</sub>(sol)<sub>2</sub>], sol = dmf [17], thf [18].

Among the above mononuclear Ni(II) complexes, the paramagnetic ( $S = 1$ ) ones have been studied with respect to their magnetic properties. The aim was to determine their Spin Hamiltonian parameters, namely the *g* tensor, as well as the axial, *D*, and rhombic, *E*, zero-field splitting (zfs) parameters [19,20]. For that endeavor, various physical methods have been applied to literature Ni(II) complexes, like magnetometry [19,21,22], as well as high-frequency and -field EPR (HFEP) [23–36], frequency domain

\* Corresponding authors.

E-mail addresses: [krzystek@magnet.fsu.edu](mailto:krzystek@magnet.fsu.edu) (J. Krzystek), [kyritsis@chem.uoa.gr](mailto:kyritsis@chem.uoa.gr) (P. Kyritsis).

magnetic resonance (FDMRS) [29,33,37,38], and magnetic circular dichroism (MCD) spectroscopy [39].

With respect to the Ni(II) complexes containing (E,E') ligands, as expected, the geometry of their first coordination sphere proved to be the determining factor in controlling the magnitude of their  $D$  parameter: The tetrahedral  $[\text{Ni}(\text{S,S})_2]$  ( $R = R' = \text{Ph}$  or  $i\text{Pr}$ ) [11] and  $[\text{Ni}(\text{Se,Se})_2]$  ( $R = R' = i\text{Pr}$ ) [40] complexes have been amenable to magnetometry but not to HFEP studies, due to their large  $D$  values, owing to first order spin-orbit coupling (SOC). This was conclusively proved by FDMRS studies on the latter, by which  $D = 45.40$  and  $E = 1.91 \text{ cm}^{-1}$  values have been determined [40]. This observation justified the compound's HFEP silence, since integer spin systems are amenable to this method only if  $D < \text{ca. } 25 \text{ cm}^{-1}$  [41].

On the other hand, pseudo-octahedral  $\text{trans}[\text{Ni}(\text{O,E})_2(\text{sol})_2]$ ,  $E = \text{S, Se}$ ;  $\text{sol} = \text{dmf, thf}$ , lacking first-order SOC, have been studied by both magnetometry [17,18] and HFEP [18], with the latter affording accurate  $D$  and  $E$  values (*vide infra*). The sign and magnitude of  $D$ , as well as the rhombicity  $E/D$ , is of paramount importance for these integer spin systems, in the context of their eventual dynamic magnetic properties. In that respect, it should be noted that a large number of multinuclear Ni(II) complexes, of various nuclearities, have been shown to exhibit slow relaxation of magnetization [42], and thus they belong to the class of multinuclear single molecule magnets (SMMs) [43–46]. On the other hand, the recently emerged class of mononuclear SMMs [47–51], contains only three Ni(II) complexes. These complexes bear either octahedral [52,53] or trigonal bipyramidal [54] coordination spheres, and they exhibit  $D < 0$  (i.e. the  $M_s = \pm 1$  is the lowest energy sub-level of the  $S = 1$  state). This property, along with a small rhombicity,  $E/D$ , of the system, are desirable characteristics to ensure SMM-like behavior. Therefore, additional studies on Ni(II) complexes of variable coordination spheres are needed, in an effort to identify new mononuclear Ni(II) SMMs.

In this work, the synthesis, as well as the X-ray crystallographic, thermogravimetric and IR spectroscopic characterization of the octahedral  $\text{trans}[\text{Ni}(\text{O,E})_2(\text{dmsO})_2]$ ,  $E = \text{S}$  (**1**),  $\text{Se}$  (**2**), complexes, is presented. HFEP studies of these  $S = 1$  systems provided accurate Spin Hamiltonian parameters, which are compared with those of their  $\text{trans}[\text{Ni}(\text{O,E})(\text{sol})_2]$ ,  $\text{sol} = \text{dmf, thf}$ , counterparts [17,18], thus making possible to further explore magnetostructural correlations in this sub-family of pseudo-octahedral Ni(II) complexes.

## 2. Experimental

### 2.1. Synthesis

All chemical reagents used were purchased from Aldrich. Solvents were dried according to standard procedures. The LH ligands  $(\text{OPPh}_2)(\text{EPPPh}_2)\text{NH}$ ,  $E = \text{S}$  or  $\text{Se}$ , their corresponding KL salts [55], as well as complexes  $[\text{Ni}(\text{O,E})_2]$ ,  $E = \text{S}$  [16],  $\text{Se}$  [17], were synthesized according to published methods.

#### 2.1.1. Synthesis of $\text{trans}[\text{Ni}(\text{O,E})_2(\text{dmsO})_2]$ , $E = \text{S, Se}$

Blue-green and dark green crystals of tetrahedral  $[\text{Ni}(\text{O,E})_2]$ ,  $E = \text{S}$  [16],  $\text{Se}$  [17], respectively, were dissolved in  $\text{dmsO}$  at room temperature, and the color of the solution was almost instantly changed to yellow. After slow evaporation of the solvent, light yellow crystals were grown in about 3–4 days, which were shown by X-ray crystallography to correspond to complexes **1** and **2**, respectively. Main IR data ( $\text{cm}^{-1}$ ): Complex **1**,  $\nu_{\text{as}}(\text{P}_2\text{N})$  1216,  $\nu(\text{PO})$  1130, 1090,  $\nu(\text{SO})$  1001,  $\nu(\text{PS})$  589; Complex **2**,  $\nu_{\text{as}}(\text{P}_2\text{N})$  1219,  $\nu(\text{PO})$  1134, 1090,  $\nu(\text{SO})$  1001,  $\nu(\text{PSe})$  560.

### 2.2. X-ray crystallography

A crystal of **1** ( $0.36 \times 0.48 \times 0.62 \text{ mm}$ ) and a crystal of **2** ( $0.22 \times 0.25 \times 0.75 \text{ mm}$ ) were taken from the mother liquor and immediately cooled to  $-113 \text{ }^\circ\text{C}$ . Diffraction measurements were made on a Rigaku R-Axis SPIDER Image Plate diffractometer using graphite monochromated  $\text{Cu K}\alpha$  radiation. Data collection ( $\omega$ -scans) and processing (cell refinement, data reduction and Empirical absorption correction) were performed using the CrystalClear program package [56]. Important crystallographic data are listed in Table 1. The structure was solved by direct methods using SHELXS-97 and refined by full-matrix least-squares techniques on  $F^2$  with SHELXL ver.2014/6 [57,58]. Further experimental crystallographic details for **1**:  $2\theta_{\text{max}} = 130^\circ$ ; reflections collected/unique/used, 19027/4228 [ $R_{\text{int}} = 0.0548$ ]/4228; 408 parameters refined;  $(\Delta/\sigma)_{\text{max}} = 0.001$ ;  $(\Delta\rho)_{\text{max}}/(\Delta\rho)_{\text{min}} = 1.111/-0.438 \text{ e}/\text{\AA}^3$ ;  $R_1/wR_2$  (for all data), 0.0478/0.1182. Further experimental crystallographic details for **2**:  $2\theta_{\text{max}} = 130^\circ$ ; reflections collected/unique/used, 29178/4318 [ $R_{\text{int}} = 0.0404$ ]/4318; 396 parameters refined;  $(\Delta/\sigma)_{\text{max}} = 0.002$ ;  $(\Delta\rho)_{\text{max}}/(\Delta\rho)_{\text{min}} = 1.154/-0.583 \text{ e}/\text{\AA}^3$ ;  $R_1/wR_2$  (for all data), 0.0357/0.0858. All hydrogen atoms were located by difference maps and were refined isotropically or were introduced at calculated positions as riding on bonded atoms. All non-hydrogen atoms were refined anisotropically. Plots of the structures were drawn using the Diamond 3 program package [59].

### 2.3. Thermogravimetric analysis

TGA diagrams were recorded on a Mettler-Toledo TGA/DSC1 instrument under a  $\text{N}_2$  flow of 50 mL/min, between room temperature and  $800 \text{ }^\circ\text{C}$ , with a  $10 \text{ }^\circ\text{C}/\text{min}$  rate.

### 2.4. IR spectroscopy

IR spectra were run in the range  $4000\text{--}200 \text{ cm}^{-1}$  on a Perkin-Elmer 883 IR spectrophotometer, as KBr discs.

### 2.5. HFEP spectroscopy

HFEP spectra were recorded using a spectrometer that has been described previously [60], with a difference of using a Virginia Diodes (Charlottesville, VA) source operating at  $13 \pm 1 \text{ GHz}$ , amplified and multiplied by a cascade of frequency multipliers.

**Table 1**  
Crystallographic data for **1** and **2**.

	<b>1</b>	<b>2</b>
Formula	$\text{C}_{52}\text{H}_{52}\text{N}_2\text{NiO}_4\text{P}_4\text{S}_4$	$\text{C}_{52}\text{H}_{52}\text{N}_2\text{NiO}_4\text{P}_4\text{S}_2\text{Se}_2$
Formula weight	1079.78	1173.58
Space group	$P2_1/n$	$P2_1/n$
$a$ ( $\text{\AA}$ )	13.3803(2)	13.4582(3)
$b$ ( $\text{\AA}$ )	9.6629(1)	9.7444(2)
$c$ ( $\text{\AA}$ )	20.7617(3)	20.7360(4)
$\alpha$ ( $^\circ$ )	90.0	90.0
$\beta$ ( $^\circ$ )	109.606(1)	108.902(1)
$\gamma$ ( $^\circ$ )	90.0	90.0
$V$ ( $\text{\AA}^3$ )	2528.70(6)	2572.72(9)
$Z$	2	2
$T$ ( $^\circ\text{C}$ )	-113	-113
Radiation	$\text{Cu K}\alpha$	$\text{Cu K}\alpha$
$\rho_{\text{calcd}}$ ( $\text{g cm}^{-3}$ )	1.418	1.515
$\mu$ ( $\text{mm}^{-1}$ )	3.672	4.469
Reflections with $I > 2\sigma(I)$	3961	4234
$R_1^a$	0.0452	0.0348
$wR_2^a$	0.1160	0.0853

<sup>a</sup>  $R_1 = \sum(|F_o| - |F_c|)/\sum(|F_o|)$  and  $wR_2 = \{\sum[w(F_o^2 - F_c^2)^2]/\sum[w(F_o^2)]\}^{1/2}$   $w = 1/[\sigma^2(F_o^2) + (aP)^2 + bP]$  and  $P = [\max(F_o^2) + 2F_c^2]/3$ ,  $a = 0.0566$ ,  $b = 3.4795$  for (**1**);  $a = 0.0330$ ,  $b = 5.9401$  for (**2**).

A visibly crystalline sample of complex **1** (19 mg) was carefully ground to obtain fine powder prior to the experiment. Because of a strong field-induced torquing effect demonstrating itself in the HFEPR spectra, the sample was subsequently immobilized in an *n*-eicosane mull. The spectra of both constrained and unconstrained forms were, however, useful and were both subject to analysis.

Complex **2** (12 mg) was powdery and did not necessitate grinding. This sample did not torque in magnetic field, either, and was therefore used 'as is' in the experiments.

### 2.5.1. Analysis of HFEPR data

The multifrequency HFEPR data obtained for complexes **1** and **2** were fitted using the Spin Hamiltonian of an  $S = 1$  system (Eq. (1)):

$$H = \beta_e B \cdot \mathbf{g} \cdot S + D[S_z^2 - S(S+1)/3] + E(S_x^2 - S_y^2) \quad (1)$$

in which the  $\mathbf{g}$  tensor represents the Zeeman interaction,  $D$  and  $E$  are, respectively, the axial and rhombic zfs components, and  $\beta_e$  is the electron Bohr magneton. A full analytical solution of the Spin Hamiltonian eigenvalue problem for the  $S = 1$  case can be found in textbooks [20].

## 3. Results and discussion

### 3.1. Synthesis

Complexes **1** and **2** were obtained by dissolving  $[\text{Ni}(\text{O},\text{E})_2]$ ,  $\text{E} = \text{S}, \text{Se}$ , in dmso, and by slow evaporation of the latter. This work extends the previously established sub-family of  $\text{trans-}[\text{Ni}(\text{O}, \text{E})_2(\text{sol})_2]$  complexes,  $\text{sol} = \text{dmf}, \text{thf}$  [17,18], which had been isolated by similar procedures.

### 3.2. X-ray crystallography

The crystal data and refinement characteristics of the structure of complexes **1** and **2** are shown in Table 1. The ORTEP representation of the crystal structures of **1** and **2** is shown in Figs. 1 and 2, respectively, and selected bond lengths and angles are listed in Table 2. Based on the unit cell parameters of the two structures (Table 1), as well as on the almost complete matching of the two structural models in the overlap mode representation of Fig. S1 (Supplementary Material, SM), compounds **1** and **2** are considered to be isomorphous. Both structures possess a center of symmetry, as

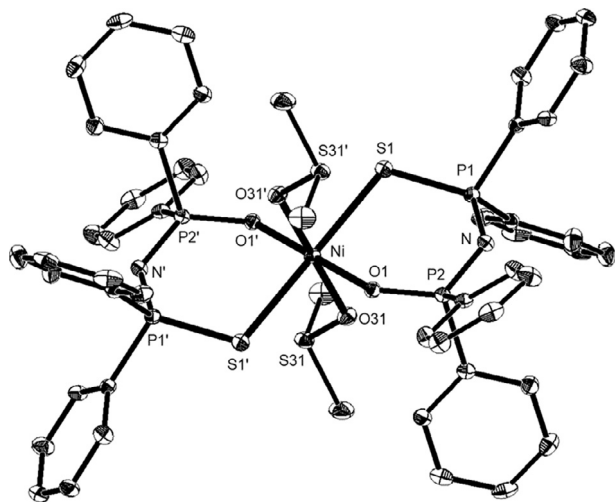


Fig. 1. ORTEP representation of complex **1** at 30% thermal probability ellipsoids. Primed atoms are generated by symmetry ( $i$ )  $2 - x, -y, 2 - z$ .

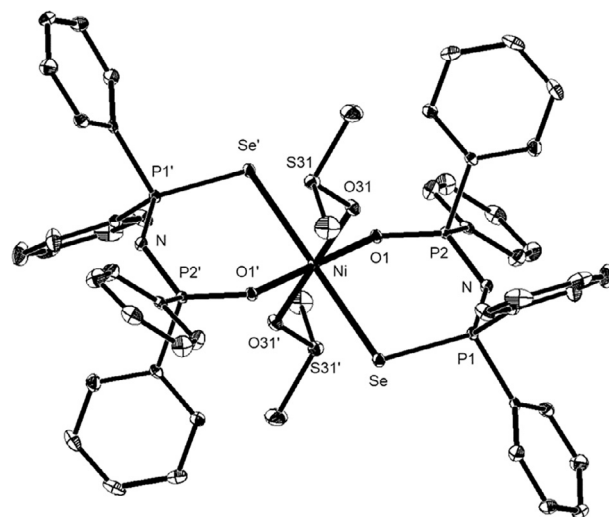


Fig. 2. ORTEP representation of complex **2** at 30% thermal probability ellipsoids. Primed atoms are generated by symmetry ( $i$ )  $2 - x, -y, 2 - z$ .

Table 2

Selected bond lengths (Å) and angles (°) for **1** and **2**.

<b>1</b>		<b>2</b>	
Distances (Å)			
Ni–O1	2.027(2)	Ni–O1	2.025(2)
Ni–O31(dmso)	2.049(2)	Ni–O31	2.054(2)
Ni–S1	2.536(2)	Ni–Se	2.629(1)
Angles (°)			
O1–Ni–O1'	180	O1–Ni–O1'	180
O1–Ni–O31'	90.19(8)	O1–Ni–O31'	90.08(8)
O1–Ni–O31	89.81(8)	O1–Ni–O31	89.92(8)
O31–Ni–O31'	180	O31–Ni–O31'	180
O1'–Ni–S1	95.13(6)	O1'–Ni–Se	95.38(5)
O1–Ni–S1	84.87(6)	O1–Ni–Se	84.62(5)
O31'–Ni–S1	92.07(6)	O31'–Ni–Se	92.18(6)
O31–Ni–S1	87.93(6)	O31–Ni–Se	87.82(6)
S1–Ni–S1'	180	Se–Ni–Se'	180

is also the case for the analogous  $\text{trans-}[\text{Ni}(\text{O},\text{E})_2(\text{sol})_2]$  complexes,  $\text{E} = \text{S}, \text{Se}$ ;  $\text{sol} = \text{dmf}$  [17],  $\text{thf}$  [18].

#### 3.2.1. Complex **1**

The crystals of complex **1** contain discrete monomeric molecules, exhibiting distorted octahedral  $\text{NiO}_4\text{S}_2$  cores, in which Ni (II) is coordinated by two equatorial (O,S) chelates in *trans* arrangement, whereas the two axial coordination sites are taken by the O atom of two dmso molecules. The two symmetry-related and therefore identical equatorial Ni–O1 and Ni–S1 bond lengths are 2.027(2) and 2.536(2) Å, respectively, with the large difference between the two values reflecting a significant deviation from the ideal octahedral geometry. On the other hand, the two axial Ni–O<sub>ax</sub>(dmso) bond lengths are 2.049(2) Å, being larger by 0.022 Å from the equatorial Ni–O1 ones. The Ni–O<sub>eq</sub> bond lengths are larger by 0.074 Å compared to the Ni–O bonds of tetrahedral  $[\text{Ni}(\text{O}, \text{S})_2]$  (average 1.953 Å) [16]. However, the Ni–S bond lengths are larger by 0.24 Å and 0.30 Å, compared, respectively, to those of  $[\text{Ni}(\text{O}, \text{S})_2]$  (average 2.296 Å) [16] and tetrahedral  $[\text{Ni}(\text{S}, \text{S})_2]$  (average 2.235 Å) [8,9], revealing a remarkable weakening of the Ni–S bonds in pseudo-octahedral complex **1**.

The equatorial Ni–O1 bonds of complex **1** [2.027(2) Å] are similar to those of  $[\text{Ni}(\text{O},\text{O})_2(\text{dmf})_2]$  (2.054 and 2.113 Å) [15],  $\text{trans-}[\text{Ni}(\text{O},\text{S})_2(\text{dmf})_2]$  (2.021 Å) [17] and  $\text{trans-}[\text{Ni}(\text{O},\text{S})_2(\text{thf})_2]$  (2.014 Å) [18] complexes. The Ni–S bond lengths of complex **1** 2.536(2) Å are also similar compared with those of the corresponding bond lengths in  $\text{trans-}[\text{Ni}(\text{O},\text{S})_2(\text{dmf})_2]$  (2.518 Å) [17] and  $\text{trans-}[\text{Ni}(\text{O},$

$S)_2(thf)_2]$  (2.534 Å) [18]. The axial Ni–O(solvent) bond lengths of *trans*-[Ni(O,S)<sub>2</sub>(sol)<sub>2</sub>], sol = dmsO [2.049(2) Å], dmF (2.068 Å) [17], thf (2.151 Å) [18], reveal a weaker Ni(II) coordination of thf compared to dmsO and dmF, confirming an appraisal of the relative coordination ability of these solvents [61].

The P–N–P angles of **1** 130.7(2)° are decreased slightly compared to the corresponding angle (132.9°) in the protonated ligand (OPPh<sub>2</sub>)<sub>2</sub>(SPPH<sub>2</sub>)NH [55]. The two equivalent P–O bond lengths [1.506(2) Å] of **1** are rather similar to the corresponding values (1.493 Å and 1.515 Å) of the two ligand molecules observed in the asymmetric unit of the corresponding crystal [55]. On the other hand, the two equivalent P–S bond lengths of **1** [1.993(1) Å] are increased by 0.08 Å compared to the average of the values (1.914 Å and 1.917 Å) in the two ligand molecules observed in the asymmetric unit of the crystal [55]. Last, the P–N bond lengths of **1** are averaged to 1.591 Å, which is smaller by 0.09 Å compared to the averaged value (1.680 Å) in the ligand. The changes in the bond lengths upon deprotonation and coordination of the ligand to the metal centre of **1** are consistent with delocalization of pi-electronic density over the Ni–O–P–N–P–S chelate rings, as has been previously discussed [2,62].

The distortion from the ideal octahedral geometry of complex **1** is also reflected by the different endocyclic (95.13°) and exocyclic (84.87°) equatorial O–Ni–S angles. The two equatorial six-membered chelating rings exhibit pseudo-chair conformations, with the Ni and N atoms being at the apices, at 0.62 and 0.26 Å, respectively.

A search in the Cambridge Structural Database (CSD) [63], showed that, besides complexes *trans*-[Ni(O,S)<sub>2</sub>(sol)<sub>2</sub>], sol = dmF [17] thf [18], a few mononuclear Ni(II) literature complexes bear similarities with complex **1**, since they contain a *trans*-NiO<sub>4</sub>S<sub>2</sub> coordination sphere [64–67].

### 3.2.2. Complex **2**

The crystals of **2** contain discrete monomeric molecules, exhibiting distorted octahedral NiO<sub>4</sub>Se<sub>2</sub> cores, in which the Ni(II) ions are coordinated by two equatorial (O,Se) chelates in *trans* arrangement, whereas the two axial coordination sites are taken by the O atom of two dmsO molecules. The equivalent equatorial Ni–O1 and Ni–Se bond lengths are 2.025(2) and 2.629(1) Å, respectively, with the even larger difference compared to **1**, reflecting a significant deviation from the ideal octahedral geometry. As in **1**, the two axial Ni–O<sub>ax</sub>(dmsO) bond lengths [2.054(2) Å] are slightly larger compared to the equatorial Ni–O ones.

The Ni–O bond lengths are larger by 0.06 Å compared to tetrahedral [Ni(O,Se)<sub>2</sub>] (average 1.961 Å) [17]. However, the Ni–Se bond lengths are larger by 0.22 Å and 0.28 Å, compared, respectively, to complex [Ni(O,Se)<sub>2</sub>] (average 2.414 Å) [17] and square-planar [Ni(Se,Se)<sub>2</sub>] (average 2.350 Å) [12], showing, as in **1**, weakening of the Ni–Se bonds in pseudo-octahedral **2**. The equatorial Ni–O and Ni–Se bond lengths of the analogous octahedral *trans*-[Ni(O,Se)<sub>2</sub>(dmF)<sub>2</sub>] complex are 2.024 and 2.633 Å, respectively [17], whereas the axial Ni–O bond lengths (2.074 Å) are by 0.02 Å larger compared to the corresponding bond lengths in **2**. In the case of the *trans*-[Ni(O,Se)<sub>2</sub>(thf)<sub>2</sub>] complex, the equatorial Ni–O and Ni–Se bond lengths are 2.001 and 2.577 Å, respectively [18], whereas the axial Ni–O bond lengths (2.140 Å) are significantly larger (by 0.086 Å), compared to those of **2** [2.054(2) Å]. Again, as it is also observed in **1**, the coordination of dmsO to Ni(II) is stronger than that of dmF or thf.

The distortion from the ideal octahedral geometry of **2** is also reflected by the different endocyclic (95.4°) and exocyclic (84.6°) equatorial O–Ni–Se angles. As in the case of **1**, the two equatorial six-membered Ni–O–P–N–P–Se chelating rings are not planar but they exhibit pseudo-chair conformations, with the Ni and N atoms at the apices, at 0.67 and 0.27 Å, respectively.

It should be noted that, besides complexes *trans*-[Ni(O,Se)<sub>2</sub>(sol)<sub>2</sub>], sol = dmF [17], thf [18], a CSD search [63] did not show any Ni(II) complex containing a *trans*-[NiO<sub>4</sub>Se<sub>2</sub>] coordination sphere. On the other hand, a 1D inorganic polymer containing a *cis*-[NiO<sub>4</sub>Se<sub>2</sub>] coordination sphere, was identified [68]. It is also of interest that the CSD search did not identify any structures in which Ni(II) is coordinated to dmsO by the latter's S donor atom.

A common feature in complexes **1** and **2** is the fact that the axial Ni–O(dmsO) bond lengths [2.049(2) and 2.054(2) Å, respectively] are larger compared with the equatorial Ni–O(chelating ligand) ones [2.027(2) and 2.025(2) Å, respectively]. The same trend has been observed in literature octahedral Ni(II) complexes bearing Ni–O(dmsO) axial and Ni–O(chelating ligand) equatorial bonds [66,69–73].

### 3.3. Thermogravimetric analysis (TGA)

Thermogravimetric measurements were conducted for complexes **1** and **2** (Figs. S2 and S3), as well as for the corresponding tetrahedral, [Ni(O,E)<sub>2</sub>] E = S, Se (Figs. S4 and S5, respectively). Compared to the latter, complexes **1** and **2** display a mass loss at temperatures close to that of free dmsO's evaporation temperature (189 °C), indicating dissociation of dmsO from their coordination sphere. Indeed, the steps observed in the TGA graphs for complexes **1** and **2** at 160 °C, correspond to a 13.4% mass loss (versus 14.5% calculated mass loss of dmsO) and 14.0% (versus 13.3% calculated mass loss of dmsO), respectively. The second and more obvious change, for both complexes, at temperatures above 350 °C is exhibited by both tetrahedral [Ni(O,E)<sub>2</sub>] and pseudo-octahedral complexes **1** and **2**, and is attributed to the decomposition of the tetrahedral complexes.

### 3.4. IR spectroscopy

The bands observed for complexes **1** and **2** in the regions 1216–1219 and 1090–1134 cm<sup>-1</sup> have been assigned to ν<sub>as</sub>(P<sub>2</sub>N) and ν(PO) stretching vibrations, respectively. In addition, the intense bands at 589 and 560 cm<sup>-1</sup> of complexes **1** and **2**, are attributed to the ν(PS) and ν(PSe) vibrations, respectively. The (OPPh<sub>2</sub>)(SPPH<sub>2</sub>)NH ligand exhibits a ν<sub>as</sub>(PNP) band at 934 cm<sup>-1</sup>, ν(P–O) bands at 1202 and 1187 cm<sup>-1</sup> and a ν(P–S) band at 626 and 613 cm<sup>-1</sup> [55]. In the case of the (OPPh<sub>2</sub>)(SePPH<sub>2</sub>)NH ligand, strong bands appear at 938, 1182–1200 and 541 cm<sup>-1</sup>, which have been assigned to ν<sub>as</sub>(P<sub>2</sub>N), ν(PO) and ν(PSe) vibrations, respectively [55]. This behavior confirms the increase in the P–N bond order and the decrease in the P–O and P–S bonds order upon coordination of the ligand to Ni(II), due to the delocalization of pi-electronic density, as previously discussed [2,62]. On the other hand, the ν(P–Se) band of complex **2** (560 cm<sup>-1</sup>) increases by 19 cm<sup>-1</sup> compared to the band (541 cm<sup>-1</sup>) of the (OPPh<sub>2</sub>)(SePPH<sub>2</sub>)NH ligand. This unexpected observation is in agreement with the reported ν(P–Se) bands of 566 and 554 cm<sup>-1</sup> of square-planar *cis*-[Pd(O,Se)<sub>2</sub>] [55]. In addition, complexes **1** and **2** exhibit also an intense band at 1001 cm<sup>-1</sup>, which is assigned to the ν(SO) vibration of Ni(II)-coordinated dmsO. It should be noted that in the IR spectrum of free dmsO, the corresponding band appears at 1060 cm<sup>-1</sup>. These data provide evidence that dmsO is coordinated to Ni(II) by its O rather than its S atom [74], as was indeed confirmed by X-ray crystallography studies of complexes **1** and **2** (*vide supra*).

### 3.5. HFEPN spectroscopy

#### 3.5.1. Complex **1**

HFEPN spectra of complex **1** studied in the loose (unconstrained) form had two important features. (a) Two very broad zero-field transitions were observed at 105 ± 5 GHz and

210 ± 10 GHz (Fig. 3). The situation in which one of the zero-field transitions in a triplet state appears nearly exactly at twice the frequency of the other corresponds to the condition  $D \cong 3E$ , i.e. near-maximum rhombicity of the zfs tensor. Because of the large width of the zero-field resonances, the zfs parameters could be at this point only approximately determined as  $|D| \cong 5.25 \text{ cm}^{-1}$  and  $E \cong 1.75 \text{ cm}^{-1}$ . (b) The spectra (Fig. 4, top trace) did not correspond to those of a powder pattern expected for a triplet state, which suggested a very strong torquing effect, with the consequence of most of the crystallites orienting themselves with the z-axis of the zfs tensor parallel to the magnetic field. Indeed, the spectra could be very well simulated as if they originated from a single crystal (Fig. 4, red trace and Fig. S6, SM). Interestingly, although the zfs tensor is almost fully rhombic, EPR sensitivity to even a small deviation from rhombicity shows in the simulations of Fig. S6, which indicate that the sign of  $D$  is in fact negative. Given the actual  $E/D$  ratio (*vide infra*), this observation has little physical value.

Immersing the sample in an *n*-eicosane mull indeed dramatically changed the spectra. Fig. 4, blue trace, shows such a spectrum. Two more spectra are shown in Fig. S7 (SM). It is evident that the torquing effect has been hindered, and the spectra correspond to those of a powder pattern. Notably, a strong  $B_{\min}$  (or “half-field”) turning point that is a signature of a triplet state and was missing in the field-aligned sample is now prominent. However, the insufficient degree to which the sample was ground shows itself by the “quasi-noise effect” and effectively obscures the other turning points of the  $S = 1$  powder pattern.

Both the loose sample and the *n*-eicosane mull show a presence of a “minority species” with zfs parameters larger than those of the dominant triplet state. The nature of that species has not been identified as yet, but it is a frequent phenomenon in many transition metal coordination complexes that were analytically proven to be of a very high purity. For this reason, such species should not be construed as an impurity, but rather as a different form of the same complex, likely due to polymorphism.

In order to accurately and precisely determine the Spin Hamiltonian parameters in **1**, we combined the resonances observed in the loose sample and those found in the constrained one into a two-dimensional map (magnetic field versus frequency) [75] which is shown in Fig. 5, together with a simulation using the best fitted parameters as in Table 3.

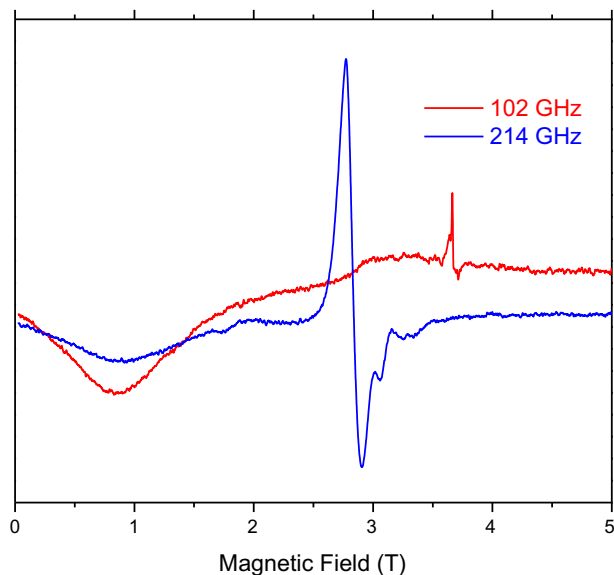


**Fig. 3.** Experimental spectra of loose complex **1** at 5 K and two indicated frequencies. Note the broad near-zero-field resonance at each frequency. The sharp signal at 3.66 T in the red spectrum originates from a  $g = 2$  impurity. (Colour online.)

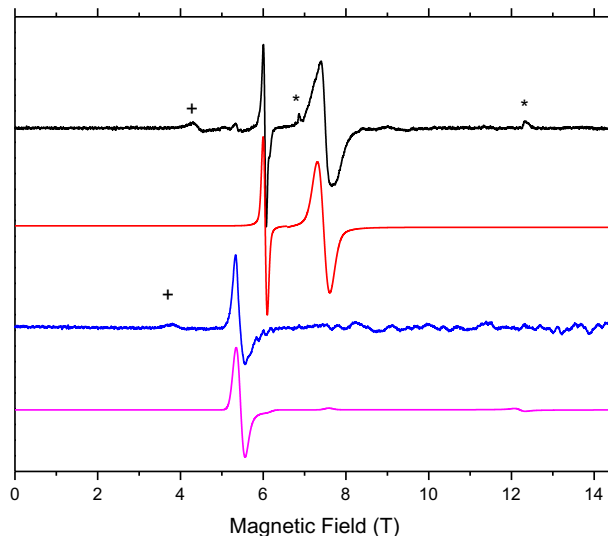


**Fig. 4.** Top: experimental spectrum of loose complex **1** at 5 K and 406.4 GHz (black trace) with a simulation (red trace) of a single crystal oriented with the magnetic field  $B_0$  in to the  $yz$  plane of the zfs tensor, using Spin Hamiltonian parameters as in Table 3. Bottom: experimental spectrum of an *n*-eicosane mull of **1** in the same conditions (blue trace) with a simulation of a powder pattern using the same Spin Hamiltonian parameters (magenta trace). The asterisks in the black spectrum denote dioxygen resonances; the plus signs in the black and blue spectra indicate a minority spin species that has not been identified. (Colour online.)

### 3.5.2. Complex 2

The sample was introduced into the magnet “as is” and produced nearly perfect powder spectra without any torquing or finite-grain effects. Therefore, it was possible to simulate the single-frequency spectra without much effort. Fig. 6 shows such a spectrum at 219 GHz and 5 K, together with simulations in two cases:  $D < 0$  and  $D > 0$ . It is apparent that the sign of  $D$  for complex **2** is positive. Spectra at two more frequencies are shown in Fig. S8 (SM).

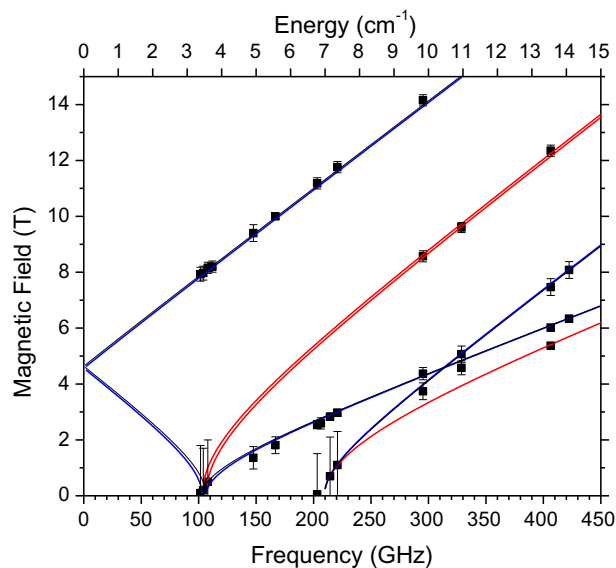


**Fig. 5.** Combined field versus frequency map of observed resonances in **1** at 5 K. Squares are experimental points; lines were drawn using the best-fitted Spin Hamiltonian parameters as in Table 3. Red lines:  $B_0||x$ , blue lines:  $B_0||y$ , black lines:  $B_0||z$ . The error bars were estimated from the peak-to-peak linewidths, which in case of near-zero-field transitions are very large. (Colour online.)

**Table 3**  
Spin Hamiltonian parameters and selected bond lengths (Å) of *trans*-[Ni(O,E)<sub>2</sub>(sol)<sub>2</sub>], E = S, Se; sol = dmso (this work), dmf [18], thf [18], as well as of literature octahedral Ni(II) complexes, determined by HFEPR at 5 K, unless otherwise stated.

Complex	Ni(II) core	Ni–O(sol)	Ni–O	Ni–E	D (cm <sup>-1</sup> )	E (cm <sup>-1</sup> )	E/D	g <sub>x</sub>	g <sub>y</sub>	g <sub>z</sub>
[Ni(O,S) <sub>2</sub> (dmso) <sub>2</sub> ]	NiO <sub>4</sub> S <sub>2</sub>	2.049	2.027	2.536	5.29(5)	1.74(1)	0.32	2.29(2)	2.29(2)	2.33 <sup>(a)</sup>
[Ni(O,Se) <sub>2</sub> (dmso) <sub>2</sub> ]	NiO <sub>4</sub> Se <sub>2</sub>	2.054	2.025	2.629	3.42(1)	0.406(5)	0.12	2.244(1)	2.248(4)	2.231(3)
[Ni(O,S) <sub>2</sub> (dmf) <sub>2</sub> ] <sup>b</sup>	NiO <sub>4</sub> S <sub>2</sub>	2.068	2.021	2.518	4.37(1)	1.23(1)	0.28	2.27(2)	2.27 <sup>(c)</sup>	2.259(6)
[Ni(O,Se) <sub>2</sub> (dmf) <sub>2</sub> ] <sup>b</sup>	NiO <sub>4</sub> Se <sub>2</sub>	2.074	2.024	2.633	3.41(1)	1.11(1)	0.33	2.230(3)	2.235(3)	2.23 <sup>(c)</sup>
[Ni(O,S) <sub>2</sub> (thf) <sub>2</sub> ] <sup>b</sup>	NiO <sub>4</sub> S <sub>2</sub>	2.151	2.014	2.534	7.11(1)	1.17(2)	0.16	2.300(6)	2.293(7)	2.306(3)
[Ni(O,Se) <sub>2</sub> (thf) <sub>2</sub> ] <sup>b</sup>	NiO <sub>4</sub> Se <sub>2</sub>	2.140	2.001	2.577	6.38(2)	1.59(2)	0.25	2.269(4)	2.289(13)	2.203(7)
[Ni(CMA) <sub>2</sub> (im) <sub>2</sub> (MeOH) <sub>2</sub> ]	NiO <sub>4</sub> N <sub>2</sub> [30] <sup>d</sup>				5.77(1)	1.636(2)	0.28	2.29(1)	2.18(1)	2.13(1)
[Ni(L <sub>1</sub> )](PF <sub>6</sub> ) <sub>2</sub>	NiO <sub>3</sub> N <sub>3</sub> [32] <sup>e</sup>				4.40	0.75	0.17	2.17	2.17	2.20
[Ni(L <sub>2</sub> )](PF <sub>6</sub> ) <sub>2</sub>	NiO <sub>3</sub> N <sub>3</sub> [32] <sup>e</sup>				4.83	0.82	0.17	2.17	2.16	2.20
[Ni(im) <sub>2</sub> (L-tyr) <sub>2</sub> ]	NiN <sub>2</sub> O <sub>2</sub> [35] <sup>f</sup>				2.997	0.4066	0.14	2.168	2.163	2.188
[Ni(HIM2-py) <sub>2</sub> NO <sub>3</sub> ]	NiO <sub>2</sub> N <sub>4</sub> [29]				10.15	0.1015	0.01	g <sub>iso</sub> = 2.17		

<sup>a</sup> g<sub>z</sub> value was obtained from the field-aligned sample.

<sup>b</sup> 10 K.

<sup>c</sup> Set, not fitted [18].

<sup>d</sup> 30 K, CMA = 9,10-dihydro-9-oxo-10-acridineacetate ion, im = imidazole.

<sup>e</sup> 7 K and 17 K, L1 = {3,4,6-tri-O-(2-picolyl)-1,2-O-ethylidene-α-D-galactopyranose}, L2 = {3,4,6-tri-O-(2-picolyl)-D-galactal}.

<sup>f</sup> L-tyr = {2-amino-3-(4-hydroxyphenyl)propanoic acid}.

Given that the single-frequency simulations were very successful, it was not necessary to employ the tunable-frequency methodology. Nevertheless, the usual 2D (field versus frequency) map of resonances [75] was collected, and the final Spin Hamiltonian parameters least-square fitted to that map (Fig. 7). The resulting values are listed in Table 3.

### 3.5.3. Magnetostructural correlations

The Spin Hamiltonian parameters of *S* = 1 *trans*-[Ni(O,E)<sub>2</sub>(sol)<sub>2</sub>], E = dmso, dmf [18], thf [18], as well as of literature octahedral Ni(II) complexes, that have been determined by HFEPR spectroscopy, are listed in Table 3, along with selected structural features of the former. Application of a multifrequency EPR approach [75] was necessary, because such integer spin systems are usually not amenable to EPR spectroscopy at conventional magnetic fields and frequencies [76]. By comparing the data for *trans*-[Ni(O,E)<sub>2</sub>(sol)<sub>2</sub>] complexes (Table 3), it seems that the total set of structural parameters of each system has a bearing on its Spin Hamiltonian parameters. However, the following initial observations can be made:

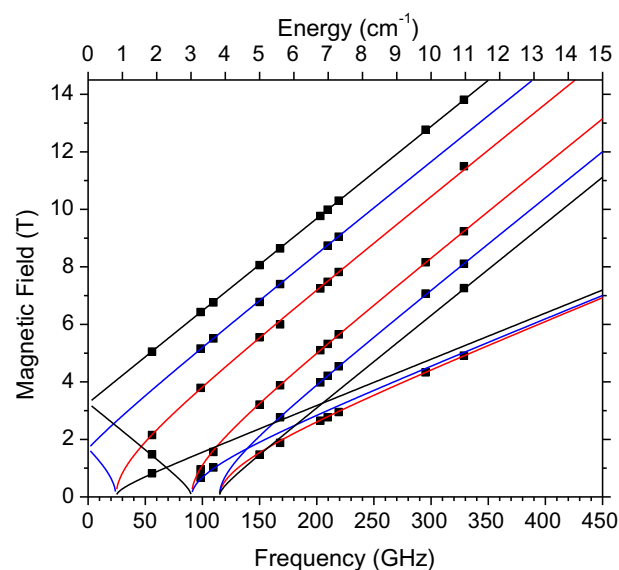


**Fig. 7.** Field versus frequency map of observed resonances in **2** at 5 K. Squares are experimental points; lines were drawn using the best-fitted spin Hamiltonian parameters as in Table 3. Red lines:  $B_0||x$ , blue lines:  $B_0||y$ , black lines:  $B_0||z$ . We did not put error bars in this figure, since the linewidths in **2** are comparable with the size of the square symbols. (Colour online.)

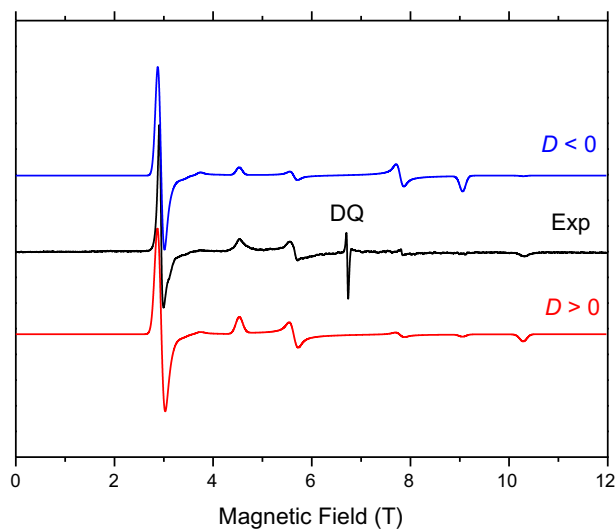


**Fig. 6.** A 219.2 GHz spectrum of **2** at 5 K. Black trace: experiment; colored traces: powder-pattern simulations using spin Hamiltonian parameters as in Table 3 for two cases:  $D < 0$  and  $D > 0$ . Blue trace: negative  $D$ ; red trace: positive  $D$ . DQ stands for a so-called “double-quantum transition”, in this case at  $g = 2.33$ , characteristic for high-spin Ni(II) and it is not simulated. (Colour online.)

- (i) Most of the complexes exhibit large rhombicities, which can be attributed to their highly anisotropic Ni(II) coordination sphere. For the extremely rhombic systems, namely *trans*-[Ni(O,S)<sub>2</sub>(dmso)<sub>2</sub>] and *trans*-[Ni(O,Se)<sub>2</sub>(dmf)<sub>2</sub>], the sign of  $D$  has no physical meaning. The rest of the *trans*-[Ni(O,E)<sub>2</sub>(sol)<sub>2</sub>] complexes listed in Table 3 were shown to exhibit  $D > 0$ . For the above reasons, it is predicted that all *trans*-[Ni(O,E)<sub>2</sub>(sol)<sub>2</sub>] complexes of Table 3 are not promising as potential mononuclear SMMs.
- (ii) For the *trans*-[Ni(O,E)<sub>2</sub>(sol)<sub>2</sub>] complexes containing sol = dmf or thf, the Se-containing one is more rhombic than its S-containing counterpart. However, this does not hold when sol = dmso, an observation that would merit additional investigation in the future, for instance by appropriate computational studies.
- (iii) For the complexes bearing the same sol, the Se-containing one exhibits slightly smaller  $D$  values compared to that of its S-containing counterpart. This behavior may be

considered as counterintuitive, if we take into account the fact that Se is heavier than S. Indeed, this observation is in contrast to the significant effects, on the magnitude of  $D$ , reported upon coordination of heavier halides to either Ni(II) [27,37,75,77] or Cr(II)/(III) [78], owing to larger SOC effects exerted by the heavier halides. With respect to effects of Se-coordination to 3d metal ions, it should be noted that similar  $D$  values have been estimated by magnetometry for  $S = 3/2$  tetrahedral  $[\text{Co}(\text{E},\text{E})_2]$  ( $\text{R} = \text{R}' = \text{iPr}$ ,  $\text{E} = \text{S}$ ,  $\text{Se}$  [79], or accurately determined by HFEPFR for  $S = 2$  tetrahedral  $[\text{Fe}(\text{E},\text{E})_2]$  ( $\text{R} = \text{R}' = \text{Ph}$ ,  $\text{E} = \text{S}$  [80]  $\text{Se}$  [81] complexes.

#### 4. Conclusions

In this work, the pseudo-octahedral  $\text{trans}-[\text{Ni}(\text{O},\text{E})_2(\text{dmsO})_2]$ ,  $\text{E} = \text{S}$ ,  $\text{Se}$ , complexes were synthesized and spectroscopically/structurally characterized, extending the previous dataset of the analogous  $\text{trans}-[\text{Ni}(\text{O},\text{E})_2(\text{sol})_2]$  complexes,  $\text{E} = \text{S}$ ,  $\text{Se}$ ;  $\text{sol} = \text{dmf}$ ,  $\text{thf}$  [18]. The six complexes of this sub-family contain  $\text{trans}-\text{NiO}_4\text{E}_2$  coordination spheres, which, however, exhibit subtle structural differences. The Ni(II) coordination of dmsO takes place via its O and not S atom, as is also the case of all structurally characterized Ni(II)-dmsO complexes reported to date. The dmsO molecules, as shown by TGA studies, are readily removed by the  $[\text{Ni}(\text{O},\text{E})_2(\text{dmsO})_2]$  coordination sphere upon heating, prior to the decomposition of the remaining tetrahedral  $[\text{Ni}(\text{O},\text{E})_2]$  complex.

The Spin Hamiltonian parameters of the  $S = 1$   $\text{trans}-[\text{Ni}(\text{O},\text{E})_2(\text{dmsO})_2]$  complexes were accurately determined by HFEPFR, making it possible to draw initial magnetostructural correlations among the sub-family of  $\text{trans}-[\text{Ni}(\text{O},\text{E})_2(\text{sol})_2]$ ,  $\text{sol} = \text{dmf}$ ,  $\text{thf}$ , complexes. The increased rhombicity in most of these complexes is attributed to their highly anisotropic coordination spheres. Furthermore, this work can trigger additional investigations by appropriate computational methods [18], which will shed more light on the structural and/or electronic factors controlling the magnetic behavior of these Ni(II) complexes.

In view of the small number of already established mononuclear Ni(II) SMMs, it is worth exploring magnetostructural correlations in additional Ni(II) complexes of variable geometries and coordination spheres.

#### Acknowledgements

E.F. has been awarded an IKY fellowship, by the act "Support for Postdoctoral Researchers", from the operational program "Human Power Development, Education and Lifelong Learning" (6, 8, 9 priority axes), co-funded by the European Social Fund and the Greek State. The HFEPFR studies were supported by the NHMFL, which is funded by the NSF (Cooperative Agreement DMR 1157490) and the State of Florida. The Fulbright Foundation in Greece and the NHMFL via its Visiting Scientist Program supported an extended scientific visit in 2013 of P.K. to the latter. Dr. Andrew Ozarowski is acknowledged for his EPR simulation and fitting program SPIN. We would like to thank all Reviewers for their constructive comments.

#### Appendix A. Supplementary data

CCDC 1831384 and 1831385 contains the supplementary crystallographic data for **1** and **2**. These data can be obtained free of charge via <http://www.ccdc.cam.ac.uk/conts/retrieving.html>, or from the Cambridge Crystallographic Data Centre, 12 Union Road, Cambridge CB2 1EZ, UK; fax: (+44) 1223-336-033; or e-mail: [deposit@ccdc.cam.ac.uk](mailto:deposit@ccdc.cam.ac.uk). Supplementary data associated with this

article can be found, in the online version, at <https://doi.org/10.1016/j.poly.2018.05.032>.

#### References

- [1] T.Q. Ly, J.D. Woollins, *Coord. Chem. Rev.* 176 (1998) 451–481.
- [2] C. Silvestru, J.E. Drake, *Coord. Chem. Rev.* 223 (2001) 117–216.
- [3] T. Chivers, J.S. Ritch, S.D. Robertson, J. Konu, H.M. Tuononen, *Acc. Chem. Res.* 43 (2010) 1053–1062.
- [4] I. Haiduc, Dichalcogenoimidodiphosphinato Ligands, in: J.A. McCleverty, T.J. Meyer (Eds.), *Comprehensive Coordination Chemistry II: From Biology to Nanotechnology*, vol. 1, Elsevier, Amsterdam, 2003, pp. 323–347.
- [5] A. Grigoropoulos, D. Maganas, D. Symeonidis, P. Giastas, A.R. Cowley, P. Kyritsis, G. Pneumatikakis, *Eur. J. Inorg. Chem.* (2013) 1170–1183.
- [6] M.R. Churchill, J. Cooke, J.P. Fennessey, J. Wormald, *Inorg. Chem.* 10 (1971) 1031–1035.
- [7] D. Cupertino, R. Keyte, A.M.Z. Slawin, D.J. Williams, J.D. Woollins, *Inorg. Chem.* 35 (1996) 2695–2697.
- [8] P. Bhattacharyya, J. Novosad, J. Phillips, A.M.Z. Slawin, D.J. Williams, J.D. Woollins, *J. Chem. Soc., Dalton Trans.* (1995) 1607–1613.
- [9] R. Rosler, C. Silvestru, G. Espinosa-Perez, I. Haiduc, R. Cea-Olivares, *Inorg. Chim. Acta* 241 (1996) 47–54.
- [10] E. Simon-Manso, M. Valderrama, D. Boys, *Inorg. Chem.* 40 (2001) 3647–3649.
- [11] D. Maganas, A. Grigoropoulos, S.S. Staniland, S.D. Chatziefthimiou, A. Harrison, N. Robertson, P. Kyritsis, F. Neese, *Inorg. Chem.* 49 (2010) 5079–5093.
- [12] C. Papadimitriou, P. Veltsistas, J. Novosad, R. Cea-Olivares, A. Toscano, P.G.Y. Garcia, M. Lopez-Cardosa, A.M.Z. Slawin, J.D. Woollins, *Polyhedron* 16 (1997) 2727–2729.
- [13] N. Levesanos, S.D. Robertson, D. Maganas, C.P. Raptopoulou, A. Terzis, P. Kyritsis, T. Chivers, *Inorg. Chem.* 47 (2008) 2949–2951.
- [14] A. Panneerselvam, C.Q. Nguyen, J. Waters, M.A. Malik, P. O'Brien, J. Raftery, M. Helliwell, *Dalton Trans.* (2008) 4499–4506.
- [15] A. Cristurean, S. Irisli, D. Marginean, C. Rat, A. Silvestru, *Polyhedron* 27 (2008) 2143–2150.
- [16] A. Silvestru, D. Bilc, R. Rosler, J.E. Drake, I. Haiduc, *Inorg. Chim. Acta* 305 (2000) 106–110.
- [17] E. Ferentinos, D. Maganas, C.P. Raptopoulou, A. Terzis, V. Psycharis, N. Robertson, P. Kyritsis, *Dalton Trans.* 40 (2011) 169–180.
- [18] D. Maganas, J. Krzystek, E. Ferentinos, A.M. Whyte, N. Robertson, V. Psycharis, A. Terzis, F. Neese, P. Kyritsis, *Inorg. Chem.* 51 (2012) 7218–7231.
- [19] R. Boča, *Coord. Chem. Rev.* 248 (2004) 757–815.
- [20] (a) A. Abragam, B. Bleaney, *Electron Paramagnetic Resonance of Transition Ions*, Dover Publications, New York, 1986; (b) N.M. Atherton, *Principles of Electron Spin Resonance*, Ellis Horwood PTR Prentice Hall, NY, 1993.
- [21] J. Titiš, R. Boča, *Inorg. Chem.* 49 (2010) 3971–3973.
- [22] R. Maurice, L. Vendier, J.-P. Costes, *Inorg. Chem.* 50 (2011) 11075–11081.
- [23] P.J. van Dam, A.A.K. Klaassen, E.J. Reijerse, W.R. Hagen, *J. Magn. Reson.* 130 (1998) 140–144.
- [24] D. Collison, M. Helliwell, V.M. Jones, F.E. Mabbs, E.J.L. McInnes, P.C. Riedi, G.M. Smith, R.G. Pritchard, W.I. Cross, *J. Chem. Soc., Faraday Trans.* 94 (1998) 3019–3025.
- [25] L.A. Pardi, A.K. Hassan, F.B. Hulsbergen, J. Reedijk, A.L. Spek, L.C. Brunel, *Inorg. Chem.* 39 (2000) 159–164.
- [26] J. Mroziński, A. Skorupa, A. Pochaba, Y. Dromzée, M. Verdager, E. Goovaerts, H. Varcammen, B. Korybut-Daszkiewicz, *J. Mol. Struct.* 559 (2001) 107–118.
- [27] J. Krzystek, J.H. Park, M.W. Meisel, M.A. Hitchman, H. Strateimer, L.C. Brunel, J. Telser, *Inorg. Chem.* 41 (2002) 4478–4487.
- [28] E.C. Yang, C. Kirman, J. Lawrence, L.N. Zakharov, A.L. Rheingold, S. Hill, D.N. Hendrickson, *Inorg. Chem.* 44 (2005) 3827–3836.
- [29] G. Røge, J.N. Rebilly, A.L. Barra, L. Sorace, G. Blondin, N. Kirchner, M. Duran, J. van Slageren, S. Parsons, L. Ricard, A. Marvilliers, T. Mallah, *Angew. Chem., Int. Ed.* 44 (2005) 1876–1879.
- [30] D. Dobrzyńska, L.B. Jerzykiewicz, M. Duczmal, A. Wojciechowska, K. Jabłońska, J. Palus, A. Ozarowski, *Inorg. Chem.* 45 (2006) 10479–10486.
- [31] P.J. Desrochers, J. Telser, S.A. Zvyagin, A. Ozarowski, J. Krzystek, D.A. Vicio, *Inorg. Chem.* 45 (2006) 8930–8941.
- [32] G. Charron, F. Bellot, F. Cisnetti, G. Pelosi, J.N. Rebilly, E. Riviere, A.L. Barra, T. Mallah, C. Polcar, *Chem. Eur. J.* 13 (2007) 2774–2782.
- [33] J.N. Rebilly, G. Charron, E. Riviere, R. Guillot, A.L. Barra, M.D. Serrano, J. van Slageren, T. Mallah, *Chem. Eur. J.* 14 (2008) 1169–1177.
- [34] I. Nieto, R.P. Bontchev, A. Ozarowski, D. Smirnov, J. Krzystek, J. Telser, J.M. Smith, *Inorg. Chim. Acta* 362 (2009) 4449–4460.
- [35] A. Wojciechowska, M. Daszkiewicz, Z. Staszak, A. Trusz-Zdybek, A. Bieńko, A. Ozarowski, *Inorg. Chem.* 50 (2011) 11532–11542.
- [36] B. Cahier, M. Perfetti, G. Zakhia, D. Naoufal, F. El-Khatib, R. Guillot, E. Riviere, R. Sessoli, A.L. Barra, N. Guihery, T. Mallah, *Chem. Eur. J.* 23 (2017) 3648–3657.
- [37] S. Vongtragool, B. Gorshunov, M. Dressel, J. Krzystek, D.M. Eichhorn, J. Telser, *Inorg. Chem.* 42 (2003) 1788–1790.
- [38] J. van Slageren, S. Vongtragool, B. Gorshunov, A.A. Mukhin, N. Karl, J. Krzystek, J. Telser, A. Muller, C. Sangregorio, D. Gatteschi, M. Dressel, *Phys. Chem. Chem. Phys.* 5 (2003) 3837–3843.
- [39] A.T. Kowal, L.C. Zambrano, I. Moura, J.J.G. Moura, J. Legall, M.K. Johnson, *Inorg. Chem.* 27 (1988) 1162–1166.

- [40] S.D. Jiang, D. Maganas, N. Levesanos, E. Ferentinos, S. Haas, K. Thirunavukkuarasu, J. Krzystek, M. Dressel, L. Bogani, F. Neese, P. Kyritsis, *J. Am. Chem. Soc.* 137 (2015) 12923–12928.
- [41] J. Krzystek, J. Telsler, *Dalton Trans.* 45 (2016) 16751–16763.
- [42] C.J. Milios, R.E.P. Winpenny, Cluster-based single-molecule magnets, in: S. Gao (Ed.), *Molecular Nanomagnets and Related Phenomena*, Springer Berlin Heidelberg, Berlin, Heidelberg, 2015, pp. 1–109.
- [43] R. Bagai, G. Christou, *Chem. Soc. Rev.* 38 (2009) 1011–1026.
- [44] G. Aromí, E.K. Brechin, Synthesis of 3d metallic single-molecule magnets, in: R. Winpenny (Ed.), *Single-Molecule Magnets and Related Phenomena*, Springer Berlin Heidelberg, Berlin, Heidelberg, 2006, pp. 1–67.
- [45] S. Goswami, A.K. Mondal, S. Konar, *Inorg. Chem. Front.* 2 (2015) 687–712.
- [46] C.J. Milios, A. Vinslava, W. Wernsdorfer, S. Moggach, S. Parsons, S.P. Perlepes, G. Christou, E.K. Brechin, *J. Am. Chem. Soc.* 129 (2007) 2754–2755.
- [47] G.A. Craig, M. Murrie, *Chem. Soc. Rev.* 44 (2015) 2135–2147.
- [48] J.M. Frost, K.L.M. Harriman, M. Murugesu, *Chem. Sci.* 7 (2016) 2470–2491.
- [49] A.K. Bar, C. Pichon, J.P. Sutter, *Coord. Chem. Rev.* 308 (2016) 346–380.
- [50] M. Atanasov, D. Aravena, E. Sutturina, E. Bill, D. Maganas, F. Neese, *Coord. Chem. Rev.* 289 (2015) 177–214.
- [51] M. Feng, M.-L. Tong, *Chem. Eur. J.* 24 (2018) 7574–7594.
- [52] (a) J. Miklovic, D. Valigura, R. Boča, J. Titiš, *Dalton Trans.* 44 (2015) 12484–12487;  
(b) J. Titiš, C. Rajnák, D. Valigura, R. Boca, *Dalton Trans.* <https://doi.org/10.1039/C8DT01445K>.
- [53] D. Lomjansky, J. Moncol, C. Rajnák, J. Titiš, R. Boča, *Chem. Commun.* 53 (2017) 6930–6932.
- [54] K.E.R. Marriott, L. Bhaskaran, C. Wilson, M. Medarde, S.T. Ochsenein, S. Hill, M. Murrie, *Chem. Sci.* 6 (2015) 6823–6828.
- [55] A.M.Z. Slawin, M.B. Smith, J.D. Woollins, *J. Chem. Soc., Dalton Trans.* (1996) 3659–3665.
- [56] M.S.C. Rigaku, CrystalClear, Rigaku/MSI Inc., The Woodlands, Texas, USA, 2005.
- [57] G.M. Sheldrick, *Acta Crystallogr., Sect. A* 64 (2008) 112–122.
- [58] G.M. Sheldrick, *Acta Crystallogr., Sect. C* 71 (2015) 3–8.
- [59] DIAMOND – Crystal and Molecular Structure Visualization, Ver. 3.1, Crystal Impact, Rathaussgasse 30, 53111, Bonn, Germany.
- [60] A.K. Hassan, L.A. Pardi, J. Krzystek, A. Sienkiewicz, P. Goy, M. Rohrer, L.C. Brunel, *J. Magn. Reson.* 142 (2000) 300–312.
- [61] R. Diaz-Torres, S. Alvarez, *Dalton Trans.* 40 (2011) 10742–10750.
- [62] D. Maganas, S.S. Staniland, A. Grigoropoulos, F. White, S. Parsons, N. Robertson, P. Kyritsis, G. Pneumatikakis, *Dalton Trans.* (2006) 2301–2315.
- [63] C.R. Groom, F.H. Allen, *Angew. Chem., Int. Ed.* 53 (2014) 662–671.
- [64] D.A. Safin, F.D. Sokolov, S.V. Baranov, L. Szyrwił, M.G. Babashkina, E.R. Shakirova, F.E. Hahn, H. Kozłowski, Z. Anorg. Allg. Chem. 634 (2008) 835–838.
- [65] A.Y. Verat, V.G. Shtyrlin, B.I. Khairutdinov, F.D. Sokolov, L.N. Yamaliev, D.B. Krivolapov, N.G. Zabirov, I.A. Litvinov, V.V. Klochkov, *Mendel. Commun.* 18 (2008) 150–152.
- [66] A.D. Bond, W. Jones, *Trans. Met. Chem.* 27 (2002) 407–410.
- [67] U. Heintz, P. Hinse, R. Frohlich, R. Mattes, *Z. Anorg. Allg. Chem.* 628 (2002) 770–778.
- [68] M.A. Petrukhina, C. Henck, B. Li, E. Block, S.-Z. Jin, R. Clerac Zhang, *Inorg. Chem.* 44 (2005) 77–84.
- [69] E. Mestrovic, I. Halasz, D.K. Bucar, M. Zgela, *Acta Crystallogr., Sect. E* 60 (2004) M367–M369.
- [70] A.M. Magerramov, R.A. Alieva, V.I. Mardanova, F.M. Chyragov, A.V. Gurbanov, K.A. Potekhin, *Russ. J. Coord. Chem.* 37 (2011) 270–274.
- [71] Z. Ma, M. Sutradhar, A.V. Gurbanov, A.M. Maharramov, R.A. Aliyeva, F.S. Aliyeva, F.N. Bahmanova, V.I. Mardanova, F.M. Chyragov, K.T. Mahmudov, *Polyhedron* 101 (2015) 14–22.
- [72] A. Djedouani, S. Boufas, A. Bendaas, M. Allain, G. Bouet, *Acta Crystallogr., Sect. E* 65 (2009) m1205–m1206.
- [73] M. Ruiz, R. Ortiz, L. Perello, A. Castineiras, M. Quiros, *Inorg. Chim. Acta* 211 (1993) 133–139.
- [74] F.A. Cotton, R. Francis, W.D. Horrocks, *J. Phys. Chem.* 64 (1960) 1534–1536.
- [75] J. Krzystek, S.A. Zvyagin, A. Ozarowski, S. Trofimenko, J. Telsler, *J. Magn. Reson.* 178 (2006) 174–183.
- [76] J. Krzystek, A. Ozarowski, J. Telsler, *Coord. Chem. Rev.* 250 (2006) 2308–2324.
- [77] R. Maurice, R. Bastardis, C. de Graaf, N. Suaud, T. Mallah, N. Guihéry, *J. Chem. Theory Comput.* 5 (2009) 2977–2984.
- [78] H.I. Karunadasa, K.D. Arquero, L.A. Berben, J.R. Long, *Inorg. Chem.* 49 (2010) 4738–4740.
- [79] S. Sottini, G. Poneti, S. Ciattini, N. Levesanos, E. Ferentinos, J. Krzystek, L. Sorace, P. Kyritsis, *Inorg. Chem.* 55 (2016) 9537–9548.
- [80] G. Mathies, S.D. Chatziefthimiou, D. Maganas, Y. Sanakis, S. Sottini, P. Kyritsis, E.J.J. Groenen, *J. Magn. Reson.* 224 (2012) 94–100.
- [81] E. Ferentinos, S. Chatziefthimiou, A.K. Boudalis, M. Pissas, G. Mathies, P. Gast, E. J.J. Groenen, Y. Sanakis, P. Kyritsis, *Eur. J. Inorg. Chem.* (2018) 713–721.